A compact core-jet structure in the changing-look Seyfert NGC 2617

Citation for the original published paper (version of record):
Yang, J., Paragi, Z., Beswick, R. et al (2021)
A compact core-jet structure in the changing-look Seyfert NGC 2617
Monthly Notices of the Royal Astronomical Society, 503(3): 3886-3895
http://dx.doi.org/10.1093/mnras/stab706

Monthly Notices of the ROYAL ASTRONOMICAL SOCIETY

MNRAS **503,** 3886–3895 (2021) doi:10.1093/mnras/stab706
Advance Access publication 2021 March 10

A compact core-jet structure in the changing-look Seyfert NGC 2617

Jun Yang [1,2★] Zsolt Paragi [2] Robert J. Beswick,[3] Wen Chen,[4] Ilse M. van Bemmel,[2] Qingwen Wu [5] Tao An [6] Xiaocong Wu,[6] Lulu Fan [7,8,9] J. B. R. Oonk,[10,11,12] Xiang Liu[13] and Weihua Wang[14]

[1]*Department of Space, Earth and Environment, Chalmers University of Technology, Onsala Space Observatory, SE-439 92 Onsala, Sweden*
[2]*Joint Institute for VLBI ERIC (JIVE), Postbus 2, NL-7990 AA Dwingeloo, the Netherlands*
[3]*Jodrell Bank Centre for Astrophysics, School of Physics and Astronomy, The University of Manchester, Manchester M13 9PL, UK*
[4]*Yunnan Observatories, Chinese Academy of Sciences, 396 Yangfangwang, Guandu District, Kunming, 650216, P. R. China*
[5]*Department of Astronomy, School of Physics, Huazhong University of Science and Technology, Wuhan 430074, China*
[6]*Shanghai Astronomical Observatory, Key Laboratory of Radio Astronomy, Chinese Academy of Sciences, 200030 Shanghai, China*
[7]*CAS Key Laboratory for Research in Galaxies and Cosmology, Department of Astronomy, University of Science and Technology of China, Hefei 230026, China*
[8]*School of Astronomy and Space Sciences, University of Science and Technology of China, Hefei 230026, China*
[9]*Shandong Provincial Key Lab of Optical Astronomy and Solar-Terrestrial Environment, Institute of Space Science, Shandong University, Weihai 264209, China*
[10]*SURFsara, PO Box 94613, NL-1090 GP Amsterdam, the Netherlands*
[11]*Leiden Observatory, Leiden University, PO Box 9513, NL-2300 RA Leiden, the Netherlands*
[12]*Netherlands Institute for Radio Astronomy (ASTRON), NL-7991 PD Dwingeloo, the Netherlands*
[13]*Xinjiang Astronomical Observatory, Key Laboratory of Radio Astronomy, Chinese Academy of Sciences, 150 Science 1-Street, 830011 Urumqi, China*
[14]*School of Computer Information Engineering, Changzhou Institute of Technology, Changzhou 213032, China*

Accepted 2021 March 5. Received 2021 March 5; in original form 2021 February 10

ABSTRACT

The nearby face-on spiral galaxy NGC 2617 underwent an unambiguous 'inside–out' multiwavelength outburst in Spring 2013, and a dramatic Seyfert-type change probably between 2010 and 2012, with the emergence of broad optical emission lines. To search for the jet activity associated with this variable accretion activity, we carried out multiresolution and multiwavelength radio observations. Using the very long baseline interferometric (VLBI) observations with the European VLBI Network at 1.7 and 5.0 GHz, we find that NGC 2617 shows a partially synchrotron self-absorbed compact radio core with a significant core shift, and an optically thin steep-spectrum jet extending towards the north up to about 2 pc in projection. We also observed NGC 2617 with the electronic Multi-Element Remotely Linked Interferometer Network at 1.5 and 5.5 GHz, and revisited the archival data of the Very Large Array (VLA) and the Very Long Baseline Array (VLBA). The radio core had a stable flux density of ∼1.4 mJy at 5.0 GHz between 2013 June and 2014 January, in agreement with the expectation of a supermassive black hole in the low accretion rate state. The northern jet component is unlikely to be associated with the 'inside–out' outburst of 2013. Moreover, we report that most optically selected changing-look active galactic nuclei (AGN) at $z < 0.83$ are sub-mJy radio sources in the existing VLA surveys at 1.4 GHz, and it is unlikely that they are more active than normal AGN at radio frequencies.

Key words: galaxies: active – galaxies: individual: NGC 2617 – galaxies: jets – galaxies: Seyfert – radio continuum: galaxies.

1 INTRODUCTION

The broad-line and continuum components of active galactic nuclei (AGN) may vary moderately (e.g. NGC 4151, Penston & Perez 1984). In the extreme cases, broad Balmer emission lines could vanish completely from Type 1 galaxies or appear from Type 2 galaxies. Recently, well-observed and extreme cases include the Seyfert galaxies NGC 2617 (Shappee et al. 2014; Oknyansky et al. 2017), Mrk 590 (Denney et al. 2014; Koay et al. 2016; Yang et al. 2021), Mrk 1018 (McElroy et al. 2016; Noda & Done 2018), X-ray AGN 1ES 1927 + 654 (e.g. Gabanyi et al. 2014; Trakhtenbrot et al. 2019; Ricci et al. 2020), and the quasar SDSS J015957.64 + 003310.5 (LaMassa et al. 2015). Moreover, the number of changing-look AGN has recently been significantly increased by some dedicated search campaigns (e.g. Runco et al. 2016; Yang et al. 2018; Frederick et al. 2019; MacLeod et al. 2019; Guo et al. 2020).

These dramatic type changes are generally interpreted as a consequence of variable accretion activity (e.g. Peterson, Korista & Cota 1986; LaMassa et al. 2015; Noda & Done 2018) rather than variable obscuring material along the line of sight. On the one hand, the scenario of the dust obscuration fails to naturally explain large variations of the mid-infrared luminosity (10 changing-look AGN, Sheng et al. 2017) and low linear polarization degrees in low ultraviolet (UV) and optical blue bands (13 changing-look quasars, Hutsemékers et al. 2019). On the other hand, a high increase in accretion rate can power stronger broad lines (e.g. Peterson et al. 1986; Elitzur, Ho & Trump 2014). There is also a positive correlation

★ E-mail: jun.yang@chalmers.se

Table 1. List of the radio flux densities of NGC 2617. Columns give (1) observing band, (2) date, (3) integrated flux density and total error including the systematic error (5 per cent for the VLA and *e*-MERLIN observations, 10 per cent for the VLBI observations), (4) map peak brightness and statistical off-source root mean square, (5) observing frequency (6) major and minor axes, position angle of synthesized beam, (7) used array (and configuration), (8) project name, and (9) reference.

Band	Date	$S_{\rm int}$ (mJy)	$S_{\rm pk}$ (mJy beam^{-1})	$\nu_{\rm obs}$ (GHz)	Synthesized beam (Major, Minor, PA)	Array	Project	Reference
L	1993 Apr 26	19.8 ± 1.0	13.6 ± 0.1	1.40	5.2×4.5 arcsec^2, $+12\overset{\circ}{.}1$	VLA:B	AT0149B	This paper
L	1993 Jul 06	24.5 ± 1.2	11.2 ± 0.1	1.43	29.4×16.1 arcsec^2, $+34\overset{\circ}{.}1$	VLA:D	AT0149D	This paper
L	1993 Nov 15	28.1 ± 1.6	21.2 ± 0.5	1.40	45.0×45.0 arcsec^2	VLA:D	NVSS	Condon et al. (1998)
L	1995 Jul 10	4.8 ± 0.3	3.2 ± 0.3	1.43	2.0×1.4 arcsec^2, $-18\overset{\circ}{.}7$	VLA:A	AM0492A	This paper
L	2013 Jun 07	1.2 ± 0.3	0.82 ± 0.05	1.67	24.7×3.7 mas^2, $+74\overset{\circ}{.}5$	EVN	RY005	This paper
L	2013 Jun 29	1.3 ± 0.2	1.25 ± 0.10	1.64	11.9×5.0 mas^2, $+4\overset{\circ}{.}4$	VLBA	SS004	This paper
L	2013 Sep 18	1.4 ± 0.1	0.85 ± 0.03	1.66	24.0×3.2 mas^2, $+77\overset{\circ}{.}0$	EVN	EY021A	This paper
L	2014 Jan 25	2.0 ± 0.2	2.15 ± 0.18	1.53	623.0×109.0 mas^2, $+19\overset{\circ}{.}9$	*e*-MERLIN	CY1026	This paper
C	2013 Jun 29	1.4 ± 0.1	1.28 ± 0.07	4.99	3.8×1.6 mas^2, $+2\overset{\circ}{.}2$	VLBA	SS004	This paper
C	2013 Oct 09	1.2 ± 0.1	1.10 ± 0.02	4.99	6.3×2.0 mas^2, $+76\overset{\circ}{.}9$	EVN	EY021B	This paper
C	2014 Jan 11	1.5 ± 0.2	1.51 ± 0.11	5.50	104.0×71.8 mas^2, $+29\overset{\circ}{.}2$	*e*-MERLIN	CY1026	This paper
X	1995 Jul 10	≤ 0.3 (3σ)	$\leq 0.3(3\sigma)$	8.44	0.33×0.23 arcsec^2, $-22\overset{\circ}{.}3$	VLA:A	AM0492A	This paper

($R_{\rm BLR} \propto L^{\rho}$, ρ in the range of 0.56–0.70) between the characteristic broad-line region size $R_{\rm BLR}$ and the Balmer emission line, X-ray, UV, and optical continuum luminosity L (Kaspi et al. 2005). If extreme changing-look phenomena represent some short, intensive, and probably episodic accretion activity of supermassive black holes (SMBHs) in the very inner accretion discs, they would be highly interesting objects for radio observations to search for short-lived jets on parsec scales (Wołowska et al. 2017; Yang et al. 2021) and to probe complex accretion–ejection activity (e.g. Marscher et al. 2002; Fender, Homan & Belloni 2009; Yuan & Narayan 2014; Blandford, Meier & Readhead 2019).

The nearby face-on galaxy NGC 2617 at $z = 0.0142$ (Paturel et al. 2003) was first identified by Moran, Halpern & Helfand (1996) as a Seyfert 1.8 spiral galaxy because of very weak broad lines. Shappee et al. (2014) reported that its central AGN had a strong multiband AGN outburst between 2013 April 24 and June 20 from X-ray to near-infrared wavelengths with increasing time lags up to ∼8 d, which can be naturally explained by the reprocessing of the inner X-ray emission. It showed a dramatic Seyfert type change from 1.8 to 1, with the appearance of broad optical emission lines. Oknyansky et al. (2017) proposed that the Seyfert-type change probably occurred between 2010 October and 2012 February.

NGC 2617 also has a radio counterpart first detected in the National Radio Astronomical Observatory (NRAO) Very Large Array (VLA) Sky Survey (NVSS; Condon et al. 1998). Its host galaxy shows significant radio emission of H I line in the H I Parkes All Sky Survey catalogue (Doyle et al. 2005). To search for short-lived, parsec-scale jets associated with the outburst and type changes, we initiated very long baseline interferometric (VLBI) imaging observations of NGC 2617. The pilot high-resolution VLBI observations found a compact structure (Yang et al. 2013) and a flat spectrum between 1.7 and 5.0 GHz (Jencson et al. 2013). The data of these pilot observations are also re-visited by us in the paper. The updated results are reported in Table 1. Moreover, we carried out follow-up dual-frequency European VLBI Network (EVN) and electronic Multi-Element Remotely Linked Interferometer Network (*e*-MERLIN) observations.

The paper is organized in the following sequence. We introduce our radio observations and data reduction in Section 2. We present our imaging results of NGC 2617 in Section 3.1. In Section 4, we interpret its parsec-scale radio morphology, investigate possible jet activity associated with the Seyfert-type change and the outburst of 2013, and discuss short-lived radio sources and the population of optically selected changing-look AGN in general. Throughout the paper, a standard ΛCDM cosmological model with $H_0 = 71$ km s^{-1} Mpc^{-1}, $\Omega_{\rm m} = 0.27$, $\Omega_{\Lambda} = 0.73$ is adopted. The VLBI images of NGC 2617 have a scale of 0.31 pc mas^{-1}. The error propagation is done via the PYTHON package UNCERTAINTY.[1]

2 OBSERVATIONS AND DATA REDUCTION

2.1 EVN observations at 1.7 and 5.0 GHz

We observed NGC 2617 with the EVN at 1.7 and 5.0 GHz in 2013. The basic experiment parameters are listed in Table 2. The participating EVN stations were Effelsberg (EF), phased-up array of the Westerbork Synthesis Radio Telescope (WB), Jodrell Bank Lovell (JB1) and MK II (JB2), Hartebeesthoek (HH), Onsala (ON), Noto (NT), Medicina (MC), Toruń (TR), and Yebes (YS). The experiments used the available maximum data rate 1024 Mbps (16 MHz filters, 2 bit quantization, 16 subbands in dual polarization). All the three experiments were carried out in the *e*-VLBI mode (Szomoru 2008). The data were streamed to Joint Institute for VLBI ERIC via broad-band fibre connections and then correlated in the real-time mode by the EVN software correlator (SFXC, Keimpema et al. 2015) using the general correlation parameters (1 or 2 s integration time, 32 or 64 points per subband) for continuum experiments.

We used J0834−0417 as the phase-referencing calibrator during the observations of NGC 2617. The calibrator has an angular separation of 16 arcmin to our target NGC 2617. The correlation position for the calibrator is RA $= 08^{\rm h}34^{\rm m}53\overset{\rm s}{.}47$, Dec. $= -04^{\circ}17'11\overset{''}{.}4$. In the phase-referencing astrometry, we took the more accurate position RA $= 08^{\rm h}34^{\rm m}53\overset{\rm s}{.}475012$, Dec. $= -04^{\circ}17'11\overset{''}{.}36845$ ($\sigma_{\rm ra} = 0.5$ mas, $\sigma_{\rm dec} = 1.2$ mas) provided by the radio fundamental catalogue 2020B (Petrov 2021). The cycle time is ∼4 min (∼40 s for J0834−0417, ∼150 s for NGC 2617, ∼40 s for two gaps). We also inserted several short scans of bright calibrators B0845−051 and 4C 39.25.

The correlation output data were calibrated with the NRAO software package Astronomical Image Processing System (AIPS, Greisen 2003). When the visibility data were loaded into AIPS discs, we excluded one quarter of side channels because of their very low

[1] https://pythonhosted.org/uncertainties/

Table 2. Configurations of the EVN and *e*-MERLIN observations of NGC 2617. The two-letter code for each station is explained in Section 2.

Project Code	Freq. (GHz)	Bandwidth (MHz)	Starting time (UT)	Duration (h)	Participating stations	Phase-referencing Quality
RY005	1.66	128	2013 Jun 07, 11h	7	EF, WB, JB1, HH, ON, NT, MC, TR	Poor
EY021A	4.99	128	2013 Sep 18, 05h	7	EF, WB, JB2, HH, ON, NT, MC, TR, YS	Successful
EY021B	1.66	128	2013 Oct 09, 03h	8	EF, WB, JB2, HH, ON, NT, MC	Successful
CY1026	5.50	512	2014 Jan 11, 21h	18	JB2, KN, PI, DA, CM, DE	Successful
CY1026	1.53	512	2014 Jan 24, 20h	9	JB2, KN, PI, DA, CM	Successful

correlation amplitude. In view of the data flagging, we re-normalized the autocorrelation and cross-correlation amplitudes of the data with the AIPS task ACCOR. Before a priori amplitude calibration via antenna gain information, the antenna system temperature data were properly smoothed to minimize their noise. When antenna system temperatures and gain curves were not available, we used nominal system equivalent flux densities and a flat gain curve to do the amplitude calibration. The task TECOR was used to remove ionospheric dispersive delays calculated according to maps of total electron content provided by global positioning system satellite observations. The phase errors associated with the antenna parallactic angle variations were removed. We corrected the instrumental phases and delays across the subbands via running fringe-fitting with a short scan of the calibrator data. After the precise phase alignment, all the subband data were combined to run fringe fitting with a solution interval of about 1 min. The sensitive station (EF or Wb) was used as the reference station. The solutions were also applied to all the related sources via a two-point linear interpolation. The bandpass calibration was performed. To run these related AIPS tasks in a script, we used the PARSELTONGUE interface (Kettenis et al. 2006).

The deconvolution was performed in DIFMAP (Shepherd, Pearson & Taylor 1994). The calibrator imaging procedure was performed through several iterations of model fitting with some delta functions, i.e. point source models, and the self-calibration in DIFMAP (Shepherd et al. 1994). This special method would allow us to obtain the best possible dynamic range image (e.g. Yang et al. 2020) in case of a poor (u, v) coverage and a complex VLBI network (e.g. Yang et al. 2021). The calibrator J0834−0417 had total flux densities ∼96 mJy at 1.7 GHz, ∼66 mJy at 5.0 GHz, and ∼96 mJy at 1.7 GHz over the three epochs. Fig. 1 shows the imaging results of the phase-referencing calibrator J0834−0417 in the last two experiments. The calibrator shows a one-sided core-jet structure at both 1.7 and 5.0 GHz. Although the (u, v) coverage is poor on the long baselines, the deconvolution method allows us to achieve a reasonable dynamic range. With the input images, we re-ran the fringe-fitting and the amplitude and phase self-calibration in AIPS. All these solutions were also transferred to the target data by the linear interpolation.

To avoid bandwidth smearing effect, we used the AIPS tasks MORIF and SPLIT to rearrange the data structure of the target source NGC 2617. The output data had a relatively high-frequency resolution of 4 MHz per intermediate frequency subband. We imaged NGC 2617 with the clean algorithm in DIFMAP. The data on the sensitive short baseline EF--WB were excluded to remove some stripes in the dirty map. Because of the strong side lobes resulting from the poor (u, v) coverage, the clean windows were carefully added and enlarged to avoid cleaning near or at the side lobes. Phase self-calibration was not used during the imaging process for NGC 2617.

Our target source NGC 2617 was detected in all the three epochs. In the first epoch, the image had a significantly high image noise level because the most sensitive station EF was not available for the first five hours. In addition, there were significant phase fluctuations on short time-scales ∼5 min, most likely because of the unstable ionosphere resulting from unexpected intense solar activity during the daytime. This problem caused a poor deconvolution and a high noise level near the target source. Thus, we failed to detect any secondary component (e.g. J in Fig. 2) near the peak feature on 2013 June 7.

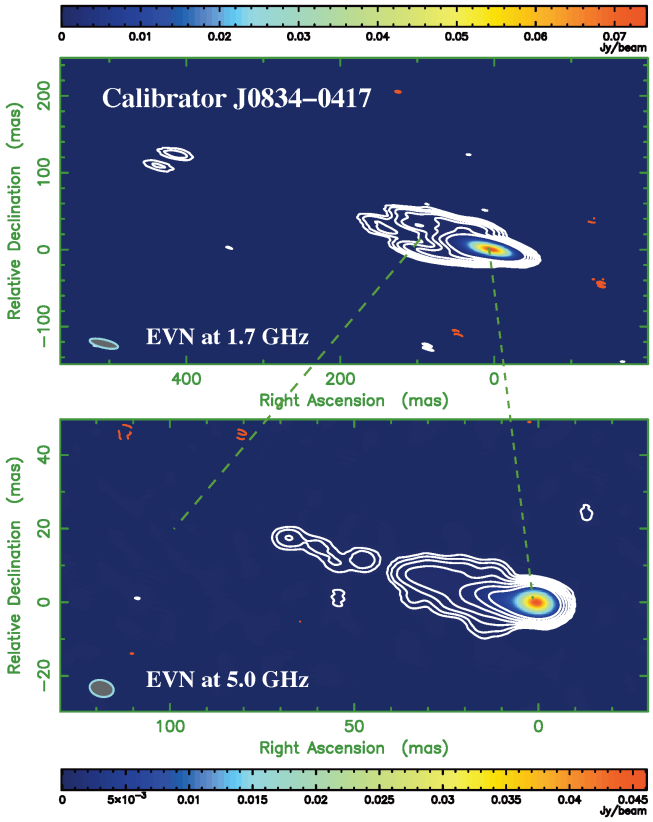

Figure 1. The total intensity images of the calibrator J0834−0417. The contours start from 3σ and increase by factors of −1, 1, 2, ..., 64. *Top*: The EVN image at 1.7 GHz. The restoring beam has a full width at half-maximum (FWHM) of 37.8 × 10.5 mas^2 at a position angle (PA) of +76.°8. The first contour is 0.027 mJy beam^{-1} and the peak brightness is 74.1 mJy beam^{-1}. *Bottom*: The EVN image at 5.0 GHz. The beam FWHM is 6.7 × 1.0 mas^2 at 79.°0. The first contour is 0.056 mJy beam^{-1} (3σ) and the peak brightness is 46.1 mJy beam^{-1}.

2.2 Broad-band *e*-MERLIN observations

We also observed NGC 2617 with the *e*-MERLIN array at *L* and *C* bands. The *C*-band observations were done with the standard frequency setup (4 subbands, 128 MHz per subband, dual polarization, 8-bit quantization). The *L*-band observations were performed with

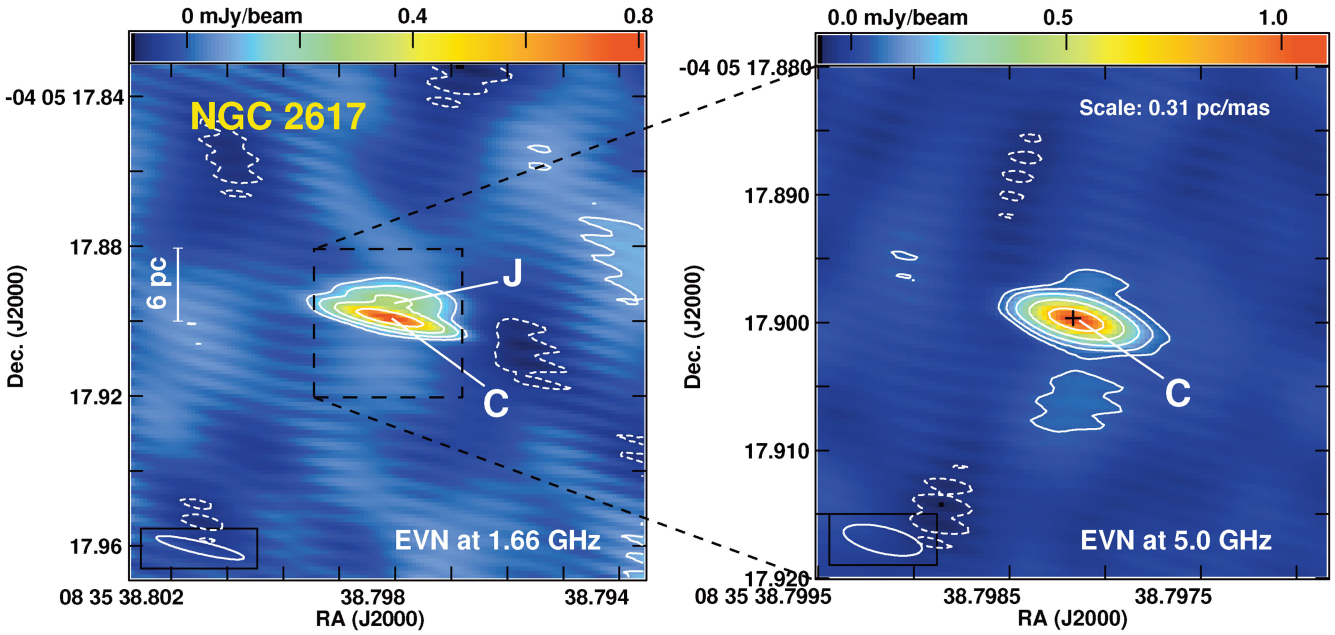

Figure 2. The faint core-jet structure found in the nearby changing-look Seyfert galaxy NGC 2617. *Left*: The EVN image at 1.66 GHz. The restoring beam FWHM is 24.0 × 3.2 mas^2 at PA = +77.°0. The contours start from 0.081 mJy beam^{-1} (2.5σ) and increase by factors of −1, 1, 2, 4, and 8. The peak brightness is 0.80 mJy beam^{-1}. *Right*: The EVN image at 5.0 GHz. The black cross denotes the optical centroid reported by the *Gaia* DR2 (second data release). The beam is 6.3 × 2.0 mas^2 at PA = 76.°9. The contours start from 0.049 mJy beam^{-1} (2.5σ) and increase by factors of −1, 1, 2, 4 and 8. The peak brightness is 1.10 mJy beam^{-1}.

the default frequency set-up (8 subbands, 64 MHz per subband, dual polarization, 2-bit quantization). The participating stations were JB2, Knocking (KN), Pickmere (PI), Darnhall (DA), Cambridge (CM), and Defford (DE). During the *L* and *C*-band experiments, the flux calibrators were 3C 286 and OQ 208, the bandpass calibrator was 0319 + 415, and the phase-referencing calibrator was J0834 − 0417.

The data were also calibrated in AIPS. First, we reviewed the data quality and flagged out very noisy data. Secondly, we did the phase and bandpass calibrations in the same way as the above EVN data reduction. Thirdly, we set the flux density of the primary flux calibrator 3C 286, ran amplitude and phase self-calibration on 3C 286, using its standard VLA image as the input source model, and treat the other calibrators as point sources. The flux density of the compact calibrator OQ 208 with respect to 3C 286 was derived using the inner three short-baseline stations, and the flux density of J0834−0417 was derived with respect to OQ 208 and using all the stations. Fourthly, we applied the self-calibration solutions and transferred the solutions from J0834−0417 to NGC 2617.

The deconvolution was done in DIFMAP. The phase calibrator J0834−0417 had a point source structure at 1.5 and 5.5 GHz. It had total flux densities 110 ± 3 mJy at 1.5 GHz and 73 ± 6 mJy at 5.5 GHz. The imaging results of NGC 2617 are reported in Table 1. We used purely natural grid weighting at *C* band, and uniform grid weighting at *L* band.

2.3 VLA and VLBA archival data

We also analysed some historical VLA data to search for the flux density variability. These experiments were observed on 1993 April 26, 1993 July 6, and 1995 July 10. We downloaded these publicly available data from the NRAO data archive[2] and reduced them step by step in the standard way recommended by the online AIPS cookbook[3] in Appendix A. The final VLA imaging results are listed in Table 1.

To make some comparisons with our EVN results, we also revisited the Very Long Baseline Array (VLBA) archival data published by Jencson et al. (2013). The data reduction followed the new calibration strategy suggested by the AIPS cookbook in appendix C. However, fringe fitting followed the EVN calibration strategy to gain more robust solutions in particular for long-baseline stations. The final VLBA imaging results are listed in Table 1.

3 MULTIRESOLUTION IMAGING RESULTS

3.1 Parsec-scale radio structure in NGC 2617

Fig. 2 displays the CLEAN maps of NGC 2617 made with purely natural grid weighting. In the low-resolution intensity image observed at 1.7 GHz on 2013 September 18, NGC 2617 displays a resolved structure, which can be decomposed into two components, C and J. The secondary component J was not detected in the 1.6-GHz VLBA maps, presented by Jencson et al. (2013) and by us in Appendix Fig. A2, because they have about three times lower sensitivity and about four times poorer resolution in the north–south direction than the EVN map (cf. Table 1). In the high-resolution image observed at 5.0 GHz on 2013 October 9, only the peak component C is clearly detected. Based on the `clean` components, NGC 2617 has total flux densities 1.47 ± 0.15 mJy at 1.7 GHz and 1.24 ± 0.13 mJy at 5.0 GHz. The uncertainties of the flux densities have included the empirical systematic errors, about 10 per cent of the flux densities.

[2] https://archive.nrao.edu/archive/advquery.jsp
[3] http://www.aips.nrao.edu/cook.html

Table 3. Summary of the circular-Gaussian model fitting results of the visibility data in DIFMAP and the related physical parameters. Columns give (1) component name reported in Fig. 2, (2) observing frequency, (3) peak brightness, (4) integrated flux density, (5–6) relative offsets in Right Ascension and Declination with respect to the peak component C (RA $= 08^{\rm h}35^{\rm m}38\overset{\rm s}{.}798152$, Dec. $= -04^{\circ}05'17\overset{''}{.}89978$, J2000, see also Table 4 and Fig. 4), (7) full width at half-maximum, i.e. de-convolved size, (8) brightness temperature, and (9) radio luminosity. The errors in columns (3–7) are the formal errors derived by the program `modelfit`. The errors in columns (8–9) are the total errors including the systematic errors (ten per cent) of flux densities.

Name	$\nu_{\rm obs}$ (GHz)	$S_{\rm pk}$ (mJy beam^{-1})	$S_{\rm int}$ (mJy)	ΔRA (mas)	ΔDec. (mas)	$\theta_{\rm size}$ (mas)	$T_{\rm b}$ (K)	$L_{\rm R}$ (erg s^{-1})
C	4.996	1.34 ± 0.02	1.21 ± 0.02	0.00 ± 0.04	0.00 ± 0.02	0.35 ± 0.06	$(4.7 \pm 1.7) \times 10^8$	$(3.0 \pm 0.3) \times 10^{37}$
C	1.662	0.90 ± 0.04	0.93 ± 0.08	0.00 ± 0.62	0.00 ± 0.19	1.56 ± 0.35	$(1.7 \pm 0.8) \times 10^8$	$(7.6 \pm 1.0) \times 10^{36}$
J	1.662	0.40 ± 0.04	0.52 ± 0.08	-3.10 ± 1.00	$+4.42 \pm 0.88$	3.46 ± 1.40	$(1.9 \pm 1.6) \times 10^7$	$(4.2 \pm 0.8) \times 10^{36}$

Table 4. List of the optical *Gaia* and the EVN 5-GHz differential astrometry results of NGC 2617. In the columns of errors, σ_f and $\sigma_{\rm s}$ represent the formal and systematic uncertainties, respectively.

Technique	Right ascension (J2000)	$\sigma_{\rm ra}$ (σ_f, $\sigma_{\rm s}$) (mas)	Declination (J2000)	$\sigma_{\rm dec}$ (σ_f, $\sigma_{\rm s}$) (mas)	Major source of $\sigma_{\rm s}$
Gaia DR2	$08^{\rm h}35^{\rm m}38\overset{\rm s}{.}798172$	$\pm0.06 \pm 0.40$	$-04^{\circ}05'17\overset{''}{.}89963$	$\pm0.06 \pm 0.40$	Extended nucleus
EVN differential astrometry	$08^{\rm h}35^{\rm m}38\overset{\rm s}{.}798152$	$\pm0.04 \pm 0.50$	$-04^{\circ}05'17\overset{''}{.}89978$	$\pm0.02 \pm 1.20$	Calibrator J0834 − 0417

Within the 3σ error bars, the total flux density measurements agree with the VLBA results. If uniform grid weighting is used, then there is a hint of a very faint ($\sim$0.2 mJy beam^{-1}) and short ($\sim$2 mas) extension towards the north in the EVN map at 5.0 GHz on 2013 October 9. The EVN map is attached in Appendix Fig. A1. However, because of its faintness ($\sim5\sigma$) and the very non-optimal (u, v) coverage of the observations, we cannot fully exclude the possibility of this being a fake structure.

To characterize the components displayed in Fig. 2, we fitted circular Gaussian models to the visibility data in DIFMAP and listed the best-fitting parameters in Table 3. The formal uncertainties are derived by the normalization of the reduced $\chi^2 = 1$. Component J is located 5.4 ± 1.0 mas (1.6 ± 0.3 pc) at PA $= -35 \pm 12$ deg from the peak component C. The component C shows a relatively compact structure at both 1.7 and 5 GHz, and has a flat radio spectrum with a spectral index of $\alpha = 0.24 \pm 0.15$. Throughout the paper, we define the α to meet the formula $S_\nu \propto \nu^\alpha$. At 5.0 GHz, the component J is not detected. This is mainly because of its steep radio spectrum and extended structure. When the 1.6-GHz image has a beam equal to that of the 5.0-GHz map, the component J has a weaker peak brightness of 0.22 mJy beam^{-1}. Using the peak brightness and 3σ as the upper limit of its peak brightness at 5.0 GHz, we could provide a constraint of $\alpha \leq -1.2$ for its peak. Similar faint steep-spectrum components are observed in other radio sources (e.g. Middelberg et al. 2004; Bontempi et al. 2012; Argo et al. 2013).

With respect to the phase-referencing calibrator J0834−0417, we measured the precise position of the peak component C at 5.0 GHz and reported the position in Table 4. Moreover, the optical *Gaia* DR2 astrometry results are also listed in Table 4. The high-precision EVN position is fully consistent with the optical *Gaia* position (Gaia Collaboration 2018). The systematic positional errors of the VLBI differential astrometry are completely dominated by the errors of the phase-referencing calibrator position. Because of the very small separation (16 arcmin) between the target and the calibrator, the systematic positional errors due to the ionospheric and tropospheric propagation effects are expected to be quite small (e.g. Reid & Honma 2014; Kirsten et al. 2015). The empirical estimate of the systematic positional error is $\sim$0.03 mas according to the five-epoch phase-referencing observations of a pair of faint calibrators with a comparable separation of 14 arcmin at 5 GHz (Mohan, An & Yang 2020).

We list brightness temperature and radio luminosity ($L_{\rm R} = \nu L_\nu$) for each component in the last two columns of Table 3. The average brightness temperature $T_{\rm b}$ is estimated (e.g. Condon et al. 1982) as

$$T_{\rm b} = 1.22 \times 10^9 \frac{S_{\rm int}}{\nu_{\rm obs}^2 \theta_{\rm size}^2}(1+z), \quad (1)$$

where $S_{\rm int}$ is the integrated flux density in mJy, $\nu_{\rm obs}$ is the observing frequency in GHz, $\theta_{\rm size}$ is the FWHM in mas, and z is the redshift. The average brightness temperature is $\sim10^8$ K. We note that the poorer angular resolution of the EVN observations in the direction east–west might overestimate $\theta_{\rm size}$ and thus underestimate $T_{\rm b}$ to some degree.

3.2 *e*-MERLIN and VLA imaging results

The *e*-MERLIN observations at 5.5 GHz show that NGC 2617 has an unresolved structure with a size of $\leq$11 mas and a total flux density of 1.5 ± 0.2 mJy on 2014 January 11 (cf. Appendix Fig. A3). Compared to the total flux densities observed early by the EVN and the VLBA at 5 GHz, we do not detect significant variability on time-scale of months.

In the *e*-MERLIN image at 1.5 GHz, Appendix Fig. A3, NGC 2617 also show a compact feature. With uniform grid weighting, the compact feature has a total flux density of 2.0 ± 0.2 mJy. This is slightly higher than the flux density found in the high-resolution VLBI observations mainly because its large beam collects some extended nuclear emission. There might also exist some very diffuse emission with a total flux density of $\sim$2 mJy mainly in the north–south direction.

The low-resolution VLA observations at 1.4 GHz reveal more diffuse radio emission with a size of 30 arcsec (Condon et al. 1982). Fig. 3 shows the diffuse structure of the central part of the host galaxy observed on 1993 April 26. In our highest angular resolution 1.4 GHz VLA data (A-configuration observations on 1995 July 10), only the central nuclear component was detected.

4 DISCUSSION

4.1 Parsec-scale core-jet structure

The pc-scale radio structure in NGC 2617 can be naturally interpreted as a faint jet powered by the central SMBH. The peak component

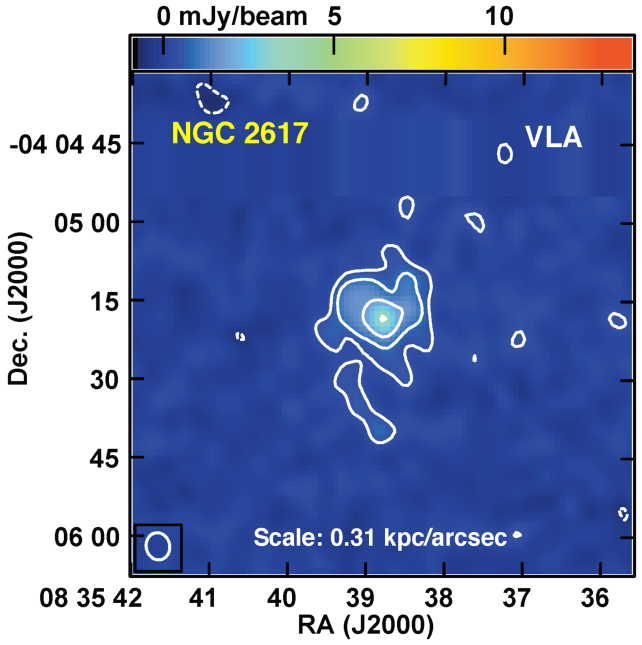

Figure 3. The 1.4-GHz image of the host galaxy of NGC 2617 derived from the VLA observation on 1993 April 26. The contours start from 0.44 mJy beam^{-1} (2.5σ) and increase by factors of -1, 1, 2, 4, and 8. Other map parameters are presented in Table 1.

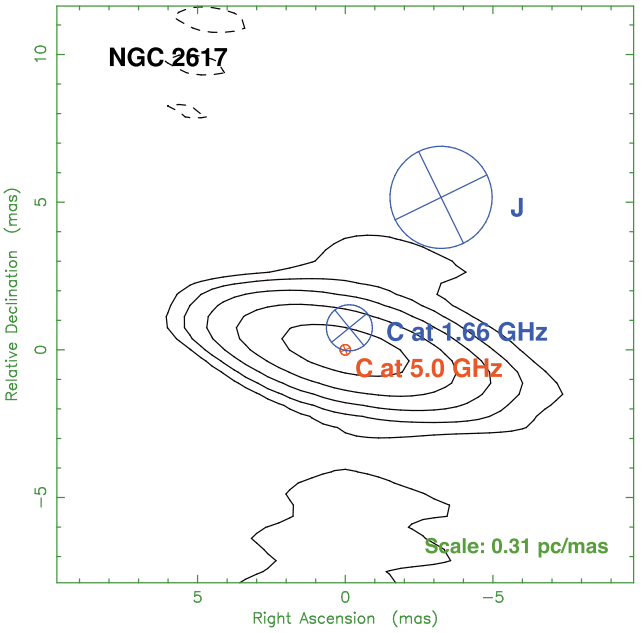

Figure 4. The frequency-dependent positional shift of the radio core in NGC 2617. These circles and their diameters represent the positions and the sizes of the best-fitting circular Gaussian models listed in Table 3.

C can be unambiguously identified as the jet base. First, it has a compact structure and a relatively flat radio spectrum (cf. Section 3.1). Secondly, the peak component C at 5.0 GHz is very close ($\sim$0.18 mas) to the centroid of the optical brightness distribution reported by *Gaia* DR2. Finally, there exists a significant frequency-dependent positional shift along the jet direction from 5.0 to 1.7 GHz. Fig. 4 shows the positional offset: $\Delta\mathrm{RA} = -0.14 \pm 0.62$ mas and $\Delta\mathrm{Dec.} = 0.75 \pm 0.19$ mas (0.23 ± 0.06 pc). Because the radio core of the phase-referencing calibrator has a jet direction along the RA, almost perpendicular to the jet direction of NGC 2617, the offset ΔDec. is mainly contributed by the radio core of NGC 2617. This offset cannot result from an apparent superluminal motion at a speed of $\sim 12c$ between the two epochs (separation: 22 d) because of its unusual moving direction (opposite to component J) and no evidence of an extremely relativistic jet. The very short interval 22 d does not allow us to explain the large offset ($\sim$0.7 light-year) as the irregular core motion, i.e. jitter (e.g. Yang et al. 2016; Rioja & Dodson 2020) because of variable opacity.

Assuming a frequency dependence of ν^{-1}, the core shift between 1.6 and 5.0 GHz is consistent with the typical value of 0.5 mas between 2.3 and 8.4 GHz observed in bright radio jets (e.g. Plavin et al. 2019; Pashchenko et al. 2020). The small angular difference $\Delta\theta$ of the radio core between two observing frequencies in a synchrotron self-absorbed jet (Blandford & Königl 1979) also scales with its radio luminosity L_R and luminosity distance D_L as $\Delta\theta \propto D_\mathrm{L}^{-1} L_\mathrm{R}^{2/3}$ (equation 3, Kovalev et al. 2008). The dependence on the radio luminosity was demonstrated during the outburst of a microquasar (Paragi et al. 2013). Compared to bright ($\gtrsim$1 Jy) one-sided jets with core shifts (e.g. Kovalev et al. 2008; Plavin et al. 2019), the jet of NGC 2617 is about three orders of magnitude fainter. However, it has a very small distance ($\sim$60 Mpc) allowing small core shifts to be studied. Within the population of mJy radio jets, these observations are among the first to detect a significant core shift. Other examples include the low-luminosity jets of M 81 that has a radio luminosity comparable to NGC 2617 and also shows a significant core shift (Martí-Vidal et al. 2011).

Component J can be naturally interpreted as a non-thermal jet component. Its radio luminosity is below the maximum luminosity, $L_\mathrm{R} \sim 10^{38.7}$ erg s^{-1}, observed in the young supernovae (Weiler et al. 2002; Varenius et al. 2019). However, it cannot be interpreted as a young supernova because there was no indication of a rapid fading phase (e.g. Varenius et al. 2019) during our multiepoch observations at *L* band. Furthermore, there was no optical supernova reported in the nucleus of the nearby face-on galaxy NGC 2617.

A core-jet structure is often seen in radio-loud Seyfert galaxies (e.g. Ulvestad 2003; Middelberg et al. 2004). The origin of radio emission from radio-quiet AGN might be star formation, an AGN-driven wind, free–free emission from photoionized gas, low-power jets, and the innermost accretion disc coronal activity (Panessa & Giroletti 2013; Panessa et al. 2019). Faint radio cores on parsec scales have been detected by VLBI observations in many galaxies (e.g. Giroletti & Panessa 2009; Bontempi et al. 2012; Park et al. 2017; Gabányi et al. 2018) and quasars (e.g. Yang et al. 2012, 2021). In the nearby changing-look Seyfert galaxy NGC 2617, the detections of the faint core-jet structure and the core shift provide more direct evidence of the collimated jet activity of the central SMBH. Moreover, compared to 280 nearby galaxies at distances $<$100 Mpc surveyed at high angular resolution with *e*-MERLIN (Baldi et al. 2018, 2021), the radio luminosity of NGC 2617 is a typical value given the distance of $\sim$60 Mpc.

4.2 Relation between jet activity, the Seyfert type change, and the outburst of 2013

In NGC 2617, there is no evidence of potential jet activity associated with the previous dramatic Seyfert-type change and the large 'inside–out' outburst of 2013 Spring. To date, there are only a few reports of jets found in changing-look AGN, such as NGC 4151 (e.g. Penston & Perez 1984; Williams et al. 2020) and Mrk 590 (Koay et al. 2016;

Yang et al. 2021). However, only Mrk 590 displayed a coincident radio outburst (Koay et al. 2016) and might have launched a short-lived jet component (Yang et al. 2021) during the 40-yr dramatic accretion activity (Denney et al. 2014).

The northern jet component J cannot result from the multiband outburst of 2013 Spring reported by Shappee et al. (2014). If it were ejected during the outburst, an apparent jet speed of $\gtrsim$10 c is expected. This inferred speed is too high for a low-power radio source (e.g. Ulvestad 2003; Kunert-Bajraszewska et al. 2010; An et al. 2012). Additionally, no radio variability was detected at 5 GHz in the radio core of NGC 2617 over our three epoch observations between 2013 June 29 and 2014 January 11, and as such there is no evidence for a radio outburst associated with the 2013 Spring multiband outburst.

The lack of relativistic ejecta in NGC 2617 might be because it failed to transfer to the high accretion rate state during the outburst. Ruan et al. (2019a) reported that NGC 2617 had a peak Eddington ratio of $\frac{L_{\rm Bol}}{L_{\rm Edd}} < 10^{-2}$. The critical value to discriminate high and low states is likely $\sim 10^{-2}$ (Ruan et al. 2019b). This is also consistent with the value observed in stellar-mass black hole X-ray binaries (e.g. McClintock & Remillard 2006). If the unified X-ray outburst model in black hole X-ray binaries (Fender et al. 2009) is applicable to extragalactic AGN (Marscher et al. 2002; Yang et al. 2021), we would expect to see a compact radio core and no episodic relativistic ejection event at the low-accretion rate state. These expectations are fully consistent with the VLBI results.

At the low accretion rate state, there exists a correlation (e.g. Merloni, Heinz & di Matteo 2003) between the radio core luminosity at 5.0 GHz, the X-ray luminosity ($L_{\rm X}$) in the 2–10 keV band, and the BH mass ($M_{\rm bh}$):

$$\log L_{\rm R} = (0.60^{+0.11}_{-0.11}) \log L_{\rm X} + (0.78^{+0.11}_{-0.09}) \log M_{\rm bh} + 7.33^{+4.05}_{-4.07}. \quad (2)$$

The central black hole in NGC 2617 has a mass of $(4 \pm 1) \times 10^7$ $M_\odot$ (Shappee et al. 2014). The X-ray luminosity was $L_{\rm X} = 10^{43.25 \pm 0.15}$ erg s^{-1} in the 2–10 keV band on 2013 April 27 and May 24 (Hernández-García et al. 2017). According to equation (2), we would expect $L_{\rm R} = 10^{39.2 \pm 1.0}$ erg s^{-1}. This estimate could be two order of magnitude higher while still in the acceptable range in view of the large scatter of the correlation and significant X-ray variability (e.g. about one order of magnitude, Shappee et al. 2014).

The Seyfert type change is estimated to have occurred between 2010 October and 2012 February (Oknyansky et al. 2017). It is not clear whether the component J was associated with this type change event. NGC 2617 was not detected ($\leq$0.3 mJy beam^{-1}) at 8.4 GHz on 1995 July 10 (Table 1). This 8.4 GHz non-detection may indicate that either the radio core has a very steep spectrum above 5 GHz, or that the core has undergone a change in flux density between 1995 and 2013 that may have coincided with the reported Seyfert-type change event. If the component J is associated with this state change event, and it keeps moving out and fading for the rest of its life, future VLBI observations would be able to detect its proper motion and variability, and then determine its birth time.

4.3 Short-lived radio sources and optically selected changing-look AGN

Most low-radio-power sources are probably short-lived jets on time-scales of $\lesssim 10^5$ yr (e.g. An & Baan 2012; Wołowska et al. 2017). Because of low accretion rates and short active phases, their jets are poorly developed and sometimes disrupted, and thus show relatively compact radio morphology. This is likely the reason why NGC 2617 has a compact core-jet structure. Recently, there are also extremely short-lived radio sources on time-scales down to a few years found in the radio surveys (e.g. Mooley et al. 2016; Kunert-Bajraszewska et al. 2020; Nyland et al. 2020). It is not clear whether short-lived radio sources are generally associated with variable accretion activity of changing-look AGN. However, since intensive accretion events may launch relativistic jets at speeds $\gtrsim$0.1 c (e.g. Marscher et al. 2002; Fender et al. 2009; Argo et al. 2015), changing-look AGN resulting from extreme accretion activity might be associated with some very short-lived radio sources (Wołowska et al. 2017; Yang et al. 2021).

Optically changing-look AGN represent unstable accretion systems. Because of variable accretions, their jets might have shorter lives than normal AGN jets. If the hypothesis is true in the local $z < 1$ Universe, this would cause a low detection rate of optically changing-look AGN at radio. Yang et al. (2018) presented a big sample of 26 optically changing-look AGN including five previously known sources at $0.08 < z < 0.58$ in the northern sky. We searched for their radio counterparts at 1.4 GHz in the NVSS catalogue (Condon et al. 1998). With an image sensitivity of $3\sigma = 1$ mJy beam^{-1} in the survey NVSS, there are only three detections: WISEA J101152.99+544206.3, WISEA J110455.17+011856.6, and FBQS J115227.5+320959. We also searched for their radio counterparts in the Faint Images of the Radio Sky at Twenty centimetre (FIRST, Becker, White & Helfand 1995) and no further sources from the sample of Yang et al. (2018) were detected despite FIRST high sensitivity. In another study including six changing-look quasars at $z \leq 0.4$ reported by Ruan et al. (2019b), none were found in the radio surveys NVSS and FIRST. In the sample of six nearby ($z \leq 0.17$) changing-look low-ionization nuclear emission-line region (LINER) galaxies (Frederick et al. 2019) that transferred from LINER galaxies to Seyfert 1 galaxies or quasars, there is only one radio detection (ZTF18aasszwr). According to these three samples, the radio detection rate of changing-look AGN is about 11 per cent (4/36). If we add five well studied nearby changing-look AGN detected in FIRST: Mrk 590 (e.g. Koay et al. 2016), Mrk 1018 (e.g. Noda & Done 2018), 1ES 1927 + 654 (e.g. Ricci et al. 2020), NGC 4151 (Williams et al. 2020), and NGC 2617, the detection rate is doubled (9/41). MacLeod et al. (2019) selected 17 changing-look quasars at $z < 0.83$ and without radio counterparts. Even withstanding the inherent selection biases of these combined studies, it is clear that the overall radio detection rate (9/58 or $\sim$16 per cent) of change-looking sources is low.

Using the VLA FIRST survey radio catalogue of 2003 April, Wadadekar (2004) searched for radio emission from $\sim$2840 AGN (from the 10th edition of the AGN catalogue, Véron-Cetty & Véron 2001) and got a detection rate of 27 per cent. The *e*-MERLIN surveys of optically selected local active (LINER and Seyfert) and inactive (H II galaxies and absorption line galaxies) galaxies gives a radio detection rate of 40 per cent for the central active SMBH (Baldi et al. 2021). Compared to the detection rates of these two larger and more complete AGN samples, the detection rate of the optically changing-look AGN is low. Moreover, we caution that flux densities from the low-resolution surveys NVSS and FIRST can be contaminated to a certain degree by star formation in host galaxies (e.g. Deller & Middelberg 2014; Herrera Ruiz et al. 2017). The above comparison of the detection rate assumes that both changing-look AGN and general AGN have very similar contamination fractions. If their contamination fractions are significant different, this would give us a systematic bias for the comparison.

Our current knowledge of the radio properties of the change-look AGN population is mainly limited by small and incomplete sample statistics. However, this apparent low radio detection rate supports the hypothesis that change-looking AGN may be short-lived radio

sources. Moreover, similar to normal AGN, the majority of changing-look AGN at $z < 0.83$ are faint sub-mJy sources at radio.

5 CONCLUSIONS

With the EVN at 1.7 and 5.0 GHz and the *e*-MERLIN at 1.5 and 5.5 GHz, we performed high-resolution radio observations of the nearby changing-look Seyfert galaxy NGC 2617 to probe its potential jet activity. We found that there exists a flat-spectrum compact radio core and a steep-spectrum jet component launched by the SMBH of NGC 2617. The one-sided jet extends towards the north up to 2 pc at 1.7 GHz and shows a core shift of 0.8 ± 0.2 mas between 1.7 and 5.0 GHz. We also re-visited the VLA and VLBA archival data. Our observations show that the radio core had no significant radio variability after the multiband 'inside–out' outburst of 2013 Spring. The northern jet might result from a much early outburst. Furthermore, we searched for radio counterparts of some changing-look AGN samples at $z \leq 0.83$ in the NVSS and FIRST catalogues, and noticed that changing-look AGN are dominated by sub-mJy radio sources and might be less active than normal AGN at radio.

ACKNOWLEDGEMENTS

TA and XW are supported by the National Key Research and Development Program of China (2018YFA0404603) and the Chinese Academy of Sciences (CAS, 114231KYSB20170003). LF acknowledges the support from the National Natural Science Foundation of China (NSFC, grant Nos. 11822303, 11773020). The EVN is a joint facility of independent European, African, Asian, and North American radio astronomy institutes. Scientific results from data presented in this publication are derived from the following EVN project code(s): RY005 and EY021. e-VLBI research infrastructure in Europe is supported by the European Commission Seventh Framework Programme (FP7/2007-2013) under grant No. RI-261525 NEXPReS. *e*-MERLIN is a National Facility operated by the University of Manchester at Jodrell Bank Observatory on behalf of STFC. The research leading to these results has received funding from the European Commission Seventh Framework Programme (FP/2007-2013) under grant No. 283393 (RadioNet3). This work has used data from the European Space Agency (ESA) mission *Gaia* (https://www.cosmos.esa.int/gaia), processed by the *Gaia* Data Processing and Analysis Consortium (DPAC, https://www.cosmos.esa.int/web/gaia/dpac/consortium). Funding for the DPAC has been provided by national institutions, in particular the institutions participating in the *Gaia* Multilateral Agreement. This research has used the NASA/IPAC Extragalactic Database (NED), which is operated by the Jet Propulsion Laboratory, California Institute of Technology, under contract with the National Aeronautics and Space Administration. This research has used NASA's Astrophysics Data System Bibliographic Services.

DATA AVAILABILITY

The correlation data underlying this article are available in the EVN data archive (http://www.jive.nl/select-experiment). The calibrated visibility data underlying this article will be shared on reasonable request to the corresponding author.

REFERENCES

An T., Baan W. A., 2012, ApJ, 760, 77
An T. et al., 2012, ApJS, 198, 5
Argo M. K., Paragi Z., Rottgering H., Klockner H. R., Miley G., Mahmud M., 2013, MNRAS, 431, L58
Argo M. K., van Bemmel I. M., Connolly S. D., Beswick R. J., 2015, MNRAS, 452, 1081
Baldi R. D. et al., 2018, MNRAS, 476, 3478
Baldi R. D. et al., 2021, MNRAS, 500, 4749
Becker R. H., White R. L., Helfand D. J., 1995, ApJ, 450, 559
Blandford R. D., Königl A., 1979, ApJ, 232, 34
Blandford R., Meier D., Readhead A., 2019, ARA&A, 57, 467
Bontempi P., Giroletti M., Panessa F., Orienti M., Doi A., 2012, MNRAS, 426, 588
Condon J. J., Condon M. A., Gisler G., Puschell J. J., 1982, ApJ, 252, 102
Condon J. J., Cotton W. D., Greisen E. W., Yin Q. F., Perley R. A., Taylor G. B., Broderick J. J., 1998, AJ, 115, 1693
Deller A. T., Middelberg E., 2014, AJ, 147, 14
Denney K. D. et al., 2014, ApJ, 796, 134
Doyle M. T. et al., 2005, MNRAS, 361, 34
Elitzur M., Ho L. C., Trump J. R., 2014, MNRAS, 438, 3340
Fender R. P., Homan J., Belloni T. M., 2009, MNRAS, 396, 1370
Frederick S. et al., 2019, ApJ, 883, 31
Gabányi K. É., Frey S., Paragi Z., Järvelä E., Morokuma T., An T., Tanaka M., Tar I., 2018, MNRAS, 473, 1554
Gabanyi K. E., Frey S., Paragi Z., An T., 2014, in 40th COSPAR Scientific Assembly. p. E1.19–36-14
Gaia Collaboration, 2018, A&A, 616, A1
Giroletti M., Panessa F., 2009, ApJ, 706, L260
Greisen E. W., 2003, in Heck A., ed., Astrophysics and Space Science Library, Vol. 285, Information Handling in Astronomy - Historical Vistas. Kluwer, Dordrecht, p. 109
Guo H. et al., 2020, ApJ, 905, 52
Hernández-García L., Masegosa J., González-Martín O., Márquez I., Guainazzi M., Panessa F., 2017, A&A, 602, A65
Herrera Ruiz N. et al., 2017, A&A, 607, A132
Hutsemékers D., Agís González B., Marin F., Sluse D., Ramos Almeida C., Acosta Pulido J. A., 2019, A&A, 625, A54
Jencson J., Kundert K., Mioduszewski A., Lucy A., Kadowaki J., Mellon S. N., 2013, Astron. Telegram, 5347, 1
Kaspi S., Maoz D., Netzer H., Peterson B. M., Vestergaard M., Jannuzi B. T., 2005, ApJ, 629, 61
Keimpema A. et al., 2015, Exp. Astron., 39, 259
Kettenis M., van Langevelde H. J., Reynolds C., Cotton B., 2006, in Gabriel C., Arviset C., Ponz D., Enrique S., eds, ASP Conf. Ser., Vol. 351, Astronomical Data Analysis Software and Systems XV. Astron. Soc. Pac., San Fransisco, p. 497
Kirsten F., Vlemmings W., Campbell R. M., Kramer M., Chatterjee S., 2015, A&A, 577, A111
Koay J. Y., Vestergaard M., Bignall H. E., Reynolds C., Peterson B. M., 2016, MNRAS, 460, 304
Kovalev Y. Y., Lobanov A. P., Pushkarev A. B., Zensus J. A., 2008, A&A, 483, 759
Kunert-Bajraszewska M., Gawroński M. P., Labiano A., Siemiginowska A., 2010, MNRAS, 408, 2261
Kunert-Bajraszewska M., Wołowska A., Mooley K., Kharb P., Hallinan G., 2020, ApJ, 897, 128
LaMassa S. M. et al., 2015, ApJ, 800, 144
MacLeod C. L. et al., 2019, ApJ, 874, 8
Marscher A. P., Jorstad S. G., Gómez J.-L., Aller M. F., Teräsranta H., Lister M. L., Stirling A. M., 2002, Nature, 417, 625
Martí-Vidal I., Marcaide J. M., Alberdi A., Pérez-Torres M. A., Ros E., Guirado J. C., 2011, A&A, 533, A111
McClintock J. E., Remillard R. A., 2006, Black Hole Binaries. Cambridge Univ. Press, Cambridge, p. 157
McElroy R. E. et al., 2016, A&A, 593, L8
Merloni A., Heinz S., di Matteo T., 2003, MNRAS, 345, 1057
Middelberg E. et al., 2004, A&A, 417, 925
Mohan P., An T., Yang J., 2020, ApJ, 888, L24
Mooley K. P. et al., 2016, ApJ, 818, 105
Moran E. C., Halpern J. P., Helfand D. J., 1996, ApJS, 106, 341

Noda H., Done C., 2018, MNRAS, 480, 3898
Nyland K. et al., 2020, ApJ, 905, 74
Oknyansky V. L. et al., 2017, MNRAS, 467, 1496
Panessa F., Giroletti M., 2013, MNRAS, 432, 1138
Panessa F., Baldi R. D., Laor A., Padovani P., Behar E., McHardy I., 2019, Nat. Astron., 3, 387
Paragi Z. et al., 2013, MNRAS, 432, 1319
Park S., Yang J., Oonk J. B. R., Paragi Z., 2017, MNRAS, 465, 3943
Pashchenko I. N., Plavin A. V., Kutkin A. M., Kovalev Y. Y., 2020, MNRAS, 499, 4515
Paturel G., Theureau G., Bottinelli L., Gouguenheim L., Coudreau-Durand N., Hallet N., Petit C., 2003, A&A, 412, 57
Penston M. V., Perez E., 1984, MNRAS, 211, 33P
Peterson B. M., Korista K. T., Cota S. A., 1986, BAAS, 18, 1001
Petrov L., 2021, AJ, 161, 14
Plavin A. V., Kovalev Y. Y., Pushkarev A. B., Lobanov A. P., 2019, MNRAS, 485, 1822
Reid M. J., Honma M., 2014, ARA&A, 52, 339
Ricci C. et al., 2020, ApJ, 898, L1
Rioja M. J., Dodson R., 2020, A&AR, 28, 6
Ruan J. J., Anderson S. F., Eracleous M., Green P. J., Haggard D., MacLeod C. L., Runnoe J. C., Sobolewska M. A., 2019a, preprint (arXiv:1909.04676)
Ruan J. J., Anderson S. F., Eracleous M., Green P. J., Haggard D., MacLeod C. L., Runnoe J. C., Sobolewska M. A., 2019b, ApJ, 883, 76
Runco J. N. et al., 2016, ApJ, 821, 33
Shappee B. J. et al., 2014, ApJ, 788, 48
Sheng Z., Wang T., Jiang N., Yang C., Yan L., Dou L., Peng B., 2017, ApJ, 846, L7
Shepherd M. C., Pearson T. J., Taylor G. B., 1994, BAAS, 26, 987
Szomoru A., 2008, in The role of VLBI in the Golden Age for Radio Astronomy. Sissa Medialab srl, Trieste, p. 40
Trakhtenbrot B. et al., 2019, ApJ, 883, 94
Ulvestad J. S., 2003, in Zensus J. A., Cohen M. H., Ros E., eds, ASP Conf. Ser., Vol. 300, Radio Astronomy at the Fringe. Astron. Soc. Pac., San Fransisco, p. 97
Varenius E. et al., 2019, A&A, 623, A173
Véron-Cetty M. P., Véron P., 2001, A&A, 374, 92
Wadadekar Y., 2004, A&A, 416, 35
Weiler K. W., Panagia N., Montes M. J., Sramek R. A., 2002, ARA&A, 40, 387
Williams D. R. A. et al., 2020, MNRAS, 495, 3079
Wołowska A., Kunert-Bajraszewska M., Mooley K., Hallinan G., 2017, Frontiers Astron. Space Sci., 4, 38
Yang J., Wu F., Paragi Z., An T., 2012, MNRAS, 419, L74
Yang J., Paragi Z., Komossa S., van Bemmel I., Oonk R., 2013, Astron. Telegram, 5125, 1
Yang J., Paragi Z., van der Horst A. J., Gurvits L. I., Campbell R. M., Giannios D., An T., Komossa S., 2016, MNRAS, 462, L66
Yang J., Gurvits L. I., Paragi Z., Frey S., Conway J. E., Liu X., Cui L., 2020, MNRAS, 495, L71
Yang J. et al., 2021, MNRAS, 502, L61
Yang J., Paragi Z., Nardini E., Baan W. A., Fan L., Mohan P., Varenius E., An T., 2021, MNRAS, 500, 2620
Yang Q. et al., 2018, ApJ, 862, 109
Yuan F., Narayan R., 2014, ARA&A, 52, 529

APPENDIX A: ADDITIONAL IMAGES

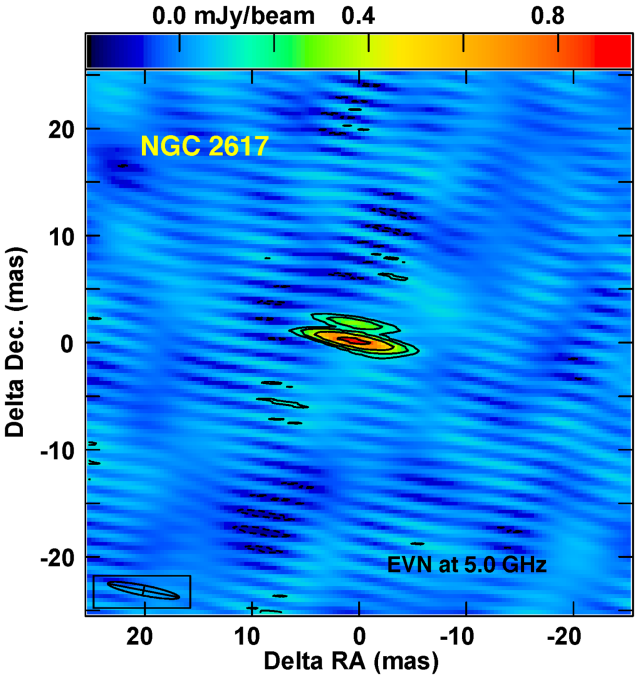

Figure A1. Hint for an inner jet component in the nearby changing-look Seyfert galaxy NGC 2617 observed by the EVN at 5 GHz with the uniform grid weighting on 2013 September 18. The contours are at the levels $2.5\sigma \times (-1, 1, 2, 4, 8)$ and $\sigma = 0.041$ mJy beam^{-1}. The map peak bright is 0.95 mJy beam^{-1}. The beam FWHM is 6.76×0.95 mas^2 at 78°.9.

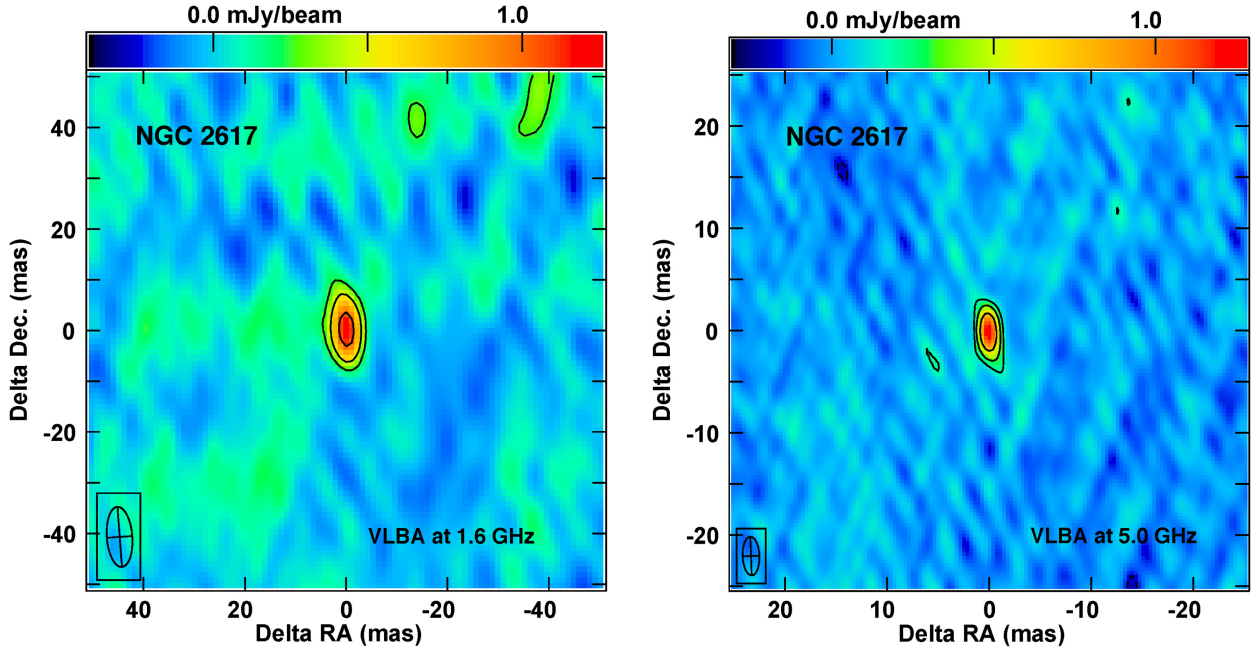

Figure A2. The compact radio morphology of the nearby changing-look Seyfert galaxy NGC 2617 observed by the VLBA at 1.6 and 5 GHz. The first contours are at the level of 2.5σ. The images were made with natural grid weighting. The map parameters are reported in Table 1.

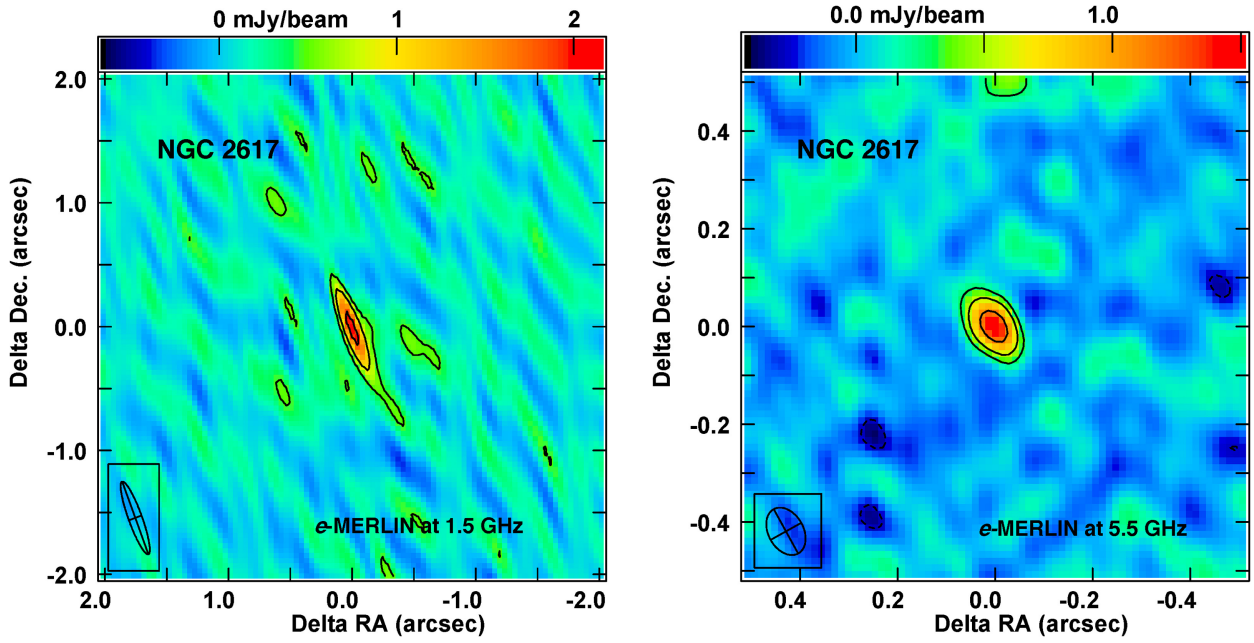

Figure A3. The compact radio structure of NGC 2617 observed by the *e*-MERLIN at 1.5 and 5.5 GHz. The first contours are at the level of 2.5σ. The images were made with uniform grid weighting at 1.5 GHz and natural grid weighting at 5.5 GHz. The map parameters are reported in Table 1.

This paper has been typeset from a TEX/LATEX file prepared by the author.